Semicond. Sci. Technol. 3 (1988) 1145–1156. Printed in the UK

REVIEW ARTICLE

The relationship of the D–X centre in $Al_xGa_{1-x}As$ and other III–V alloys with the conduction band structure

Pallab Bhattacharya

Solid State Electronics Laboratory and Centre for High Frequency Microelectronics, Department of Electrical Engineering and Computer Science, The University of Michigan, Ann Arbor, MI 48109-2122, USA

Received 14 March 1988, in final form 13 June 1988, accepted for publication 4 August 1988

Abstract. The electrical properties of the $Al_xGa_{1-x}As$ alloys for $x \geq 0.24$ are dominated by deep donors which appear in undoped and doped crystals. The corresponding defects, which are now more commonly known as D–X centres, also behave as electron traps. The properties of these defects in undoped and doped alloys are reviewed. Results of Hall, transient capacitance, deep-level transient spectroscopy and thermally stimulated capacitance measurements on crystals grown by liquid phase epitaxy and molecular beam epitaxy are presented and discussed. The deep levels have a constant thermal activation energy of 0.21 eV in the direct band-gap region, while in the same composition range the defect binding energy, as determined from Hall measurements, increases monotonically. Beyond the crossover region, the thermal activation energy and binding energy assume similar values and both decrease monotonically with increase of x. These energy values and the electron capture properties of the defects can be consistently explained by involving the interaction of the defects with indirect L and X minima. Defects with similar properties are also identified in other alloy systems in which the L and X conduction minima are lowest in energy.

1. Introduction

The $Al_xGa_{1-x}As$ ternary alloys are being extensively investigated not only for their application in heterostructure optoelectronic and microwave devices, but also for the interest in their intrinsic material properties and the physical mechanisms involved therein. The band structure of the alloys as a function of composition has now been fairly well established and has emerged from the work of several investigators, using different techniques [1–7]. The alloys have a direct band gap for $0 \leq x \leq 0.43$ and an indirect band gap for $x > 0.43$, where the X conduction minima are lowest in energy. In addition, the L conduction minima cross over with the X minima at $x = 0.37$ and with the Γ minimum at $x = 0.47$. The conduction band structure as a function of AlAs content, x, with the valence band Γ_{15v} as the reference for energy, is depicted in figure 1. More recent work [8, 9] indicates that the direct–indirect crossover at low temperatures may be at a lower value of x. However, in the context of the present paper, the Γ–L energy separation is a more important parameter. Such a dramatically changing band structure has a marked influence on the electrical and optical properties of the alloy system and properties hitherto unobserved in large band-gap binary semiconductors have been detected.

A feature which is rather unique in the ternary crystals grown by liquid phase epitaxy (LPE), molecular beam epitaxy (MBE) and metal–organic chemical vapour deposition (MOCVD) is the emergence of an electron trap level which dominates the electrical properties of the alloys with $x \geq 0.24$. The electron trap was originally identified in n-doped LPE crystals [10], and it was found that the defect concentration was proportional to the shallow donor concentration and the defect behaved in a decidely non-effective mass way. Therefore, the name D–X centre [10] has been associated with this defect to account for this dual observation. This model is supported by the observed chemical shifts in the ionisation energies dependent on the donor atom species [11, 12] and from the symmetry of the defects determined from absorption and scattering of ballistic phonons [13]. Since its identification in

0268-1242/88/121145+12 $02.50

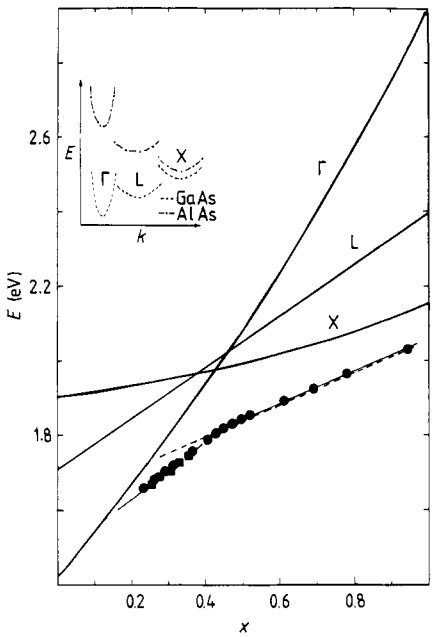

Figure 1. The conduction band structure at 300 K and the energy position of defect levels in LPE $Al_xGa_{1-x}As$. (●) from analysis of deep-level thermal emission and capture data; (■) from analysis of capacitance–voltage data; and the broken line represents the defect energy profile as calculated from the L–X hybridisation model. The thermal activation energy $\Delta E_T = 0.21 \pm 0.01$ eV in the range $0.25 \leqslant x \leqslant 0.36$ is measured with respect to the L minima and for $x > 0.36$ with respect to the X minima.

the alloys more than a decade ago, its microscopic structure has been investigated and debated by several groups of workers, but still remains unclear.

Degradations in the performance of heterostructure lasers [14] and modulation doped field-effect transistors (MODFETS) [15] have been clearly identified with the presence of the D–X centres. Since both devices use heavily doped n-type alloys, most of the investigations on the microstructure and physico-chemical origin have been made with $Al_xGa_{1-x}As$ doped with Si, S, Se and Te. It is also of importance to study the properties of the electron traps in nominally undoped crystals, in which the net electron concentration is $\simeq 10^{15}$–10^{16} cm^{-3}. Although the general features of the deep-level defects are very similar in undoped and doped LPE $Al_xGa_{1-x}As$, some differences have been observed in their electrical properties. It is believed that these differences are related to the physico–chemical origin of the centres.

In this paper, I will steer away from the microstructure and origin issues and dwell instead on another very important aspect—the relation of the defects to the band structure. I will also discuss the lattice-relaxation effect exhibited by this trap. The results of capacitance–voltage and transient capacitance measurements will be presented, in particular, to show direct evidence of the relation of the traps to the indirect band structure in the alloys. The results also confirm the band structure, and in particular, the Γ–L energy separation. The results will be discussed in the light of more recent findings. Relevant Hall, photoluminescence and photoionisation cross section data will also be presented and discussed. Finally, the presence of similar centres in InAlAs/InP alloys, and their relation to the indirect minima will also be described and discussed.

2. Electrical and optical properties of undoped liquid phase epitaxial $Al_xGa_{1-x}As$

2.1. Electrical transport properties

Experiments have been made on undoped liquid phase epitaxial (LPE) $Al_xGa_{1-x}As$ grown in our laboratories and at the Standard Telecommunication Laboratories in England on Cr-doped semi-insulating GaAs or Si-doped conducting GaAs and having thicknesses of 5–10 μm and carrier concentrations of $(5–15) \times 10^{15}$ cm^{-3}. This background electron concentration in the undoped samples originates from unidentified donor species. The range of variation of the measured carrier concentration mainly results from the minimum in the electron density around the crossover composition due to the redistribution of electrons amongst the different minima with varying effective masses. The AlAs content, x, of the layers used for the experiments in this study varied from 0.19 to 0.78 and were determined by converting measured room-temperature cathodoluminescence and photoluminescence band-gap energies into compositions from the data of Panish [16].

When Hall measurements are performed on n-type samples of $Al_xGa_{1-x}As$ as a function of temperature, the profile of the Hall electron concentration, n_H, as a function of inverse temperature shows a sharp decrease with lowering of temperature. This occurs just below 250 K and indicates a trapping of electrons from the conduction band to deep centres in the forbidden gap. Figure 2 depicts typical variations of inverse Hall coefficient, $1/eR_H$, with inverse temperature for two alloy compositions. Similar behaviour has been observed both in undoped [17] and intentionally doped [18, 19] crystals in the composition range $0.2 \leqslant x \leqslant 0.8$. A detailed analysis of the Hall effect data using a multi-conduction band model [17] yields the binding energy of the defect centres with respect to the conduction band edge and their concentration. The latter parameter has a value nearly equal to the total electron concentration, showing that the defect level plays a dominant role in contributing electrons to the conduction band. The same is true for the doped crystals [18]. The striking feature is that the binding energy changes with composition: it increases monotonically for $x \geqslant 0.25$, reaches a maximum near the band crossover composition region, and then decreases monotonically.

Figure 3 shows the defect binding energies in undoped crystals [17, 20] and in intentionally doped crystals as determined by SpringThorpe *et al* [19] (Te), Kaneko *et al* [21] (Sn), Nelson [18] (Te), Balland *et al*

[22] (Sn) and Dingle *et al* [6] (Te). It is appropriate to make some comments regarding the methods used in the determination of these binding energies. The data for the undoped n-type crystals were obtained by the methods outlined above with a fairly accurate knowledge of the conduction band structure. The data of SpringThorpe *et al*, and Nelson were obtained directly from the slope of the linear portions of the $1/eR_H - 1/T$ Hall effect data. Kaneko and co-workers obtained their data from a two-band (Γ–X) analysis of Hall effect data, ignoring the presence of the L minima. The data of Balland and co-workers were obtained from the slope of the p–n junction capacitance decay with decreasing temperature. The binding energies were obtained by Dingle and co-workers from the analysis of photoluminescence data. It is evident from the data that there is a marked difference in the binding energies determined for the apparently similar defects in undoped and intentionally doped crystals. The difference in binding energies is thought to result from the differences in the local potential of different chemical species, as observed by Lang and Logan [11] and Kumagai *et al* [12]. However, the common feature is that the binding energies goes through a maximum near the Γ-L–X crossover region due to the proximity and superposition of Bloch waves from the Γ, L, and X minima. It will be shown later that a simple model, originating from the tight binding approximation adequately describes this behaviour.

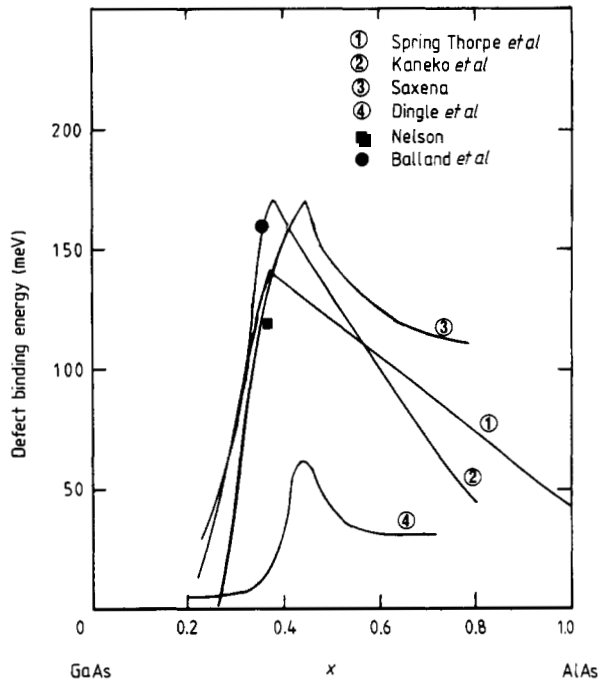

Figure 3. Variation of defect binding energy with composition in nonintentionally and intentionally doped crystals as determined by different workers. (①), (②), (③) and (■) were obtained from Hall effect data; (④) was derived from photoluminescence measurements; and (●) was derived from capacitance measurements. (③) was obtained from measurements on undoped crystals; the rest of the data presented in the figure were obtained from intentionally doped crystals.

2.2. Thermally stimulated capacitance measurements: persistent photoconductivity effects

Measurements were made on Schottky barriers fabricated on the epitaxial layers by evaporating 300–500 Å circular Au films with $(1–2)\times10^{-3}$ cm^2 area. Ohmic contacts were provided by an Ag–Sn eutectic alloy. For the measurements to be described, the samples were mounted on a cryostat holder in which the temperature could be varied from 77–500 K. These measurements were performed in order to gain a qualitative understanding of the emptying and filling of the defect centres with lowering of temperature and application of different bias voltages to the diode. The depletion layer capacitance of the diode during the different cycles of measurement was monitored by a 1 MHz meter and was recorded on an *X–Y* plotter. The typical cycle of measurement was as follows. With zero bias or a reverse bias of $\simeq 5$ V applied to the diode, the temperature was lowered from 300 to 80 K. This constitutes step 1 and for all the compositions this step was found to be reversible, i.e. the capacitance profile was retraced when the sample temperature was increased again. Next a forward bias of $\simeq 1.0$ V was applied to the diode at room temperature and the temperature was lowered. At the low-temperature limit of this step (80 K), the bias was switched back to zero and the temperature gradually raised in steps. This constitutes step 2. Finally, at the low temperature end of step 1, the sample was irradiated with 1.1 eV light when an increase in capacitance was usually observed. At this point step 3 was recorded by gradually raising the temperature of the sample to 300 K. The capacitance–temperature profiles which describe the typical behaviour in four composition ranges are depicted in figure 4. These composition ranges are: (i) $x<0.24$ where the deep level is not detected by DLTS; (ii) $0.25\leqslant x\leqslant 0.36$,

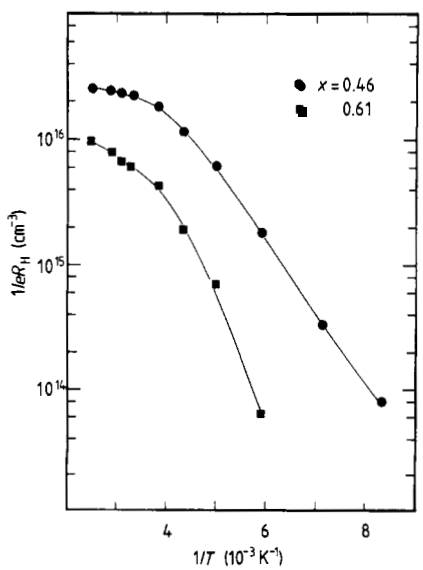

Figure 2. Variations of the inverse Hall coefficient $1/eR_H$ with temperature for two alloy compositions. The data were taken with the samples in the dark.

where the binding energy of the level monotonically increases, but the thermal activation energy remains constant; (iii) $0.37 \leqslant x \leqslant 0.50$, where the conduction valleys come close to each other in energy and eventually cross over and the depth of the level reaches a maximum; and (iv) $x > 0.50$, the indirect band-gap region where the binding energy and thermal activation energy of the level monotonically decrease. For the sample with $x = 0.19$ the capacitance values for the three steps coincide throughout the temperature range and there is no change with application of a forward bias or irradiation. This confirms that the defects are absent and the slight lowering of capacitance with lowering temperature is because of the change in the position of the Fermi level and partial filling of the shallow donors and a change in the dielectric constant. For the sample with $x = 0.25$, the capacitance profiles for the three steps can be separately seen. For $x = 0.47$ there is a sharp fall in capacitance with lowering of temperature, and no change is observed for the crystal with $x = 0.78$, but the slope of the capacitance change has decreased. There are several important features to be noted in these curves. The largest slope for the capacitance change is observed in the sample with $x = 0.47$. This confirms that amongst the four compositions the deep level has the largest binding energy at $x = 0.47$. A distinct capacitance profile for step 2 is seen only for $x = 0.25$ and not in the samples with higher values of x. It may be remembered that the low-temperature limit of step 2 denotes the condition when all the centres are filled with the application of a forward bias. Step 3 is most pronounced for the sample with $x = 0.47$. This step represents the thermal quenching of persistent photoconductivity exhibited by these centres. After the centres are optically emptied by irradiation at 80 K, a barrier is presented to electron recapture and can be overcome only by providing thermal energy. Finally, the value of the diode capacitance at 80 K for step 1 (or step 2 if it is observed) progressively decreases from $x = 0.19$ to 0.78, where it attains a very low value. This indicates an increased dominance of the deep level, into which carriers freeze out, in determining the concentration of electrons in the conduction band. For $x = 0.19$, where the diode capacitance is still high at 80 K, most of the electrons in the conduction minimum come from shallow donors which remain ionised. The experimental observations outlined above can be consistently explained by the following model. When the deep electron trap is present, the Fermi level at room temperature is close to and just below it in the forbidden energy gap. With the lowering of temperature, the Fermi level moves closer to the conduction band, thereby partially ($x = 0.25$) or completely ($x = 0.47$ and 0.78) filling the level with electrons. In the latter event, no more centres can be filled with the application of a forward bias and a separate profile for step 2 will not be observed. Lang *et al* [10] have performed similar experiments with Te-doped LPE $Al_xGa_{1-x}As$ where a large difference in capacitance was observed between steps 1 and 2 in the low-temperature limit. Consequently, in the Te-doped samples there is possibly a lesser dominance of shallow donors, and probably a larger compensation, both of which would fix the equilibrium Fermi level lower in energy in the forbidden gap. Thus a lowering of temperature is not sufficient to fill all the D–X centres. The important results obtained from these experiments are: (i) the slope of the capacitance change with lowering of temperature is related to the presence and the binding energy of the deep level; (ii) a persistent photoconductivity effect, as observed earlier in doped crystals, is also present in undoped crystals; (iii) a definite energy barrier is presented to electrons for capture by the deep centres. Lang *et al* [10] had explained this in terms of a large lattice-relaxation model. It will be shown in the next section that the results can also be explained in terms of capture via the L minima.

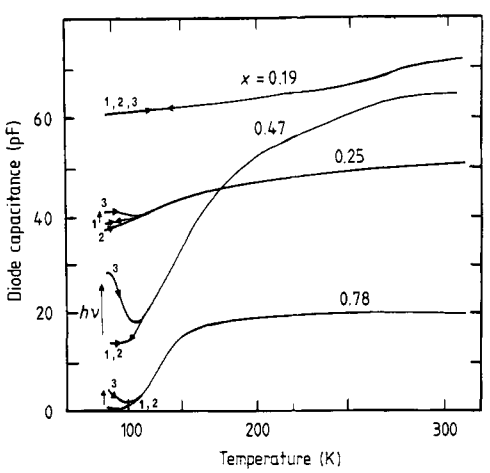

Figure 4. Thermally stimulated capacitance data for undoped samples of LPE $Al_xGa_{1-x}As$ with varying compositions. The significance of the different steps has been outlined in the text.

2.3. Low-temperature photoluminescence measurements

Deep level traps are usually non-radiative. However, it has been reported by Gaj *et al* [23] that a deep donor level in $GaAs_{1-x}P_x$ which dominated the electrical properties of the alloy near the direct to indirect band-gap transition region, participated in radiative transition processes. Other deep-level defects in this alloy system labelled BI and BII with energies 0.5 and 0.75 eV, respectively, below the conduction band edge $GaAs_{0.6}P_{0.4}$ have also been shown to be radiative centres [24, 25]. It has been established by Metz [25] that the E3 donor level identified by Lang [26] in electron-irradiated $Al_xGa_{1-x}As$ for $0 \leqslant x \leqslant 0.25$ is, at least in part, associated with a radiative centre. It is, therefore, of interest to determine whether the D–X centres in $Al_xGa_{1-x}As$ are radiative or non-radiative.

The low-temperature photoluminescence of the alloy system shows the excitonic peak and the edge luminescence as reported by Dingle *et al* [6] for

undoped and Te-doped $Al_xGa_{1-x}As$ alloys. The character of this edge luminescence varies widely throughout the composition range. Analysis of the luminescence data as a function of excitation intensity shows the presence of deep-level accptors which participate in radiative transitions, and DLTS measurements identify the same acceptors as hole traps. Contrary to the findings in $GaAs_{1-x}P_x$, it is found that the deep-donor (or electron-trap) levels, at least in the undoped crystals, do not participate in radiative transitions.

3. Emission and capture properties of D–X centres

Since the Γ–L inter-valley energy, $\Delta E_{\Gamma L}$, in $Al_xGa_{1-x}As$ changes with x, this alloy system provides a natural vehicle to study the interaction of traps with different conduction minima. With this in mind, careful transient capacitance and deep-level transient spectroscopy (DLTS) measurements were made to understand the emission and capture properties of the D–X centres and their association with the varying conduction band structure. The measurements were performed on Au Schottky diodes described previously.

Carrier capture measurements on $Al_xGa_{1-x}As$ are analysed in detail and are correlated with the emission characteristics of these traps. It will be seen that when the conduction minima with which a trap interacts are identified, a consistent picture of the emission and capture properties can be drawn and, furthermore, agreement is obtained with the results deduced from thermal equilibrium Hall effect measurements.

3.1. A model for trap emission and capture

The total depletion layer width $X=W$ of a reverse-biased Schottky barrier on n-type material in the presence of traps with energy depth E_T (measured from the lowest conduction band edge) is divided into two regions, with lengths λ and $L=W-\lambda$, by the intersection of the trap level and the Fermi level E_F. Then, the band bending energy V_L at $X=\lambda$ is related to E_T by [27]:

$$E_T = qV_L + E_F \tag{1}$$

and the excess voltage V_e associated with the trap density N_T for $0<X<\lambda$ is

$$V_e^{1/2} = A(\epsilon q N_T/2)^{1/2}(C_W^{-1} - C_L^{-1}) \tag{2}$$

where $C_W=\epsilon A/W$ is the measured diode capacitance and $C_L=\epsilon A/L$, and A is the diode area. V_e is determined from a set of voltage measurements at constant capacitance when the traps are full for $0<X<W$ and empty for $0<X<\lambda$. Also

$$V_L = C_L^{-2}\,dV/dC_s^{-2} \tag{3}$$

where C_s represents the depletion layer capacitance when the traps are full for $0<X<W$. According to equation (2), a plot of $V_e^{1/2}$ against C_W^{-1} determines C_L accurately without using the values of A or ϵ which might introduce errors. Thus V_L, and finally E_T at the measurements temperature, are accurately known by using equations (3) and (1), respectively, to within the dispersion of the Fermi distribution. At the same time, the value of N_T is determined from the slope of the plot of V_e^{-1} against C_W^{-1}.

The thermal emission constant e_n from a trap level to non-spherical conduction band minima can be expressed by [27]:

$$e_n/T^2 = \varepsilon_n \exp[-(\Delta E_T^0 + \Delta E_B)/kT] \tag{4}$$

and

$$\varepsilon_n = 3.26\times10^{21} g_n \sigma_\infty^e [(m_d/m_0)^{3/2}/(m_c/m_0)^{1/2}] \exp(\alpha/k) \quad s^{-1}K^{-2} \tag{5}$$

where $\Delta E_T=\Delta E_T^0-\alpha T$ is the activation energy of the trap, α its temperature coefficient, σ^e (cm^2) $=\sigma_\infty^e \exp(-\Delta E_B/kT)$ is the thermally activated emission cross section with barrier energy ΔE_B, g_n is the degeneracy factor, m_d and m_c are the density of states mass and the conductivity mass, respectively. The thermal velocity of carriers has been included in equations (4) and (5) as $v_T \simeq (3kT/m_c)^{1/2}$. A plot of T^2/e_n against $1/T$ yields $\Delta E_e=\Delta E_T^0+\Delta E_B$ and ε_n. If ΔE_B is known, ΔE_T^0 together with E_T (obtained from equation (1)), define the final state in the conduction band of an emission transition.

The capture constant, c (s^{-1}), of electrons by traps is related to the electron capture cross section σ^c by

$$c = \sigma^c v_+^\xi n_\xi \tag{6}$$

where n_ξ is the concentration of electrons in the $\xi=\Gamma$, L or X conduction band minima and v_T^ξ is the thermal velocity of electron in the corresponding minimum.

In a typical DLTS experiment, c is obtained from [28]

$$1-\Delta C(t_c)/\Delta C(\infty) = \exp(-ct_c), \tag{7}$$

where t_c is the trap filling time and $\Delta C(\infty)$ is the peak value of the normalised DLTS signal at a given temperature T. The slope of the plot of c against $1/T$ determines the activation energy for carrier capture. The corresponding values of σ^c at different temperatures may be determined by using equation (6) and thus σ_∞^c and ΔE_B, given by $\sigma^c=\sigma_\infty^c \exp(-\Delta E_B/kT)$, may be determined from a plot of σ^c against $1/T$ if the temperature dependence of n_ξ is known.

3.2. Experimental results

Figure 5 shows the emission activation energy plots for electron traps detected in LPE $Al_xGa_{1-x}As$ with $0.25\leqslant x\leqslant 0.36$ [29]. Electron traps were not detected for $x\leqslant 0.25$. For the indicated range of x the centres are characterised by the same emission activation energy $\Delta E_e=0.210\pm0.005$ eV and a monotonically decreasing value of ε_n with increasing AlAs content, x. Identical results are obtained with aluminium Schottky diodes.

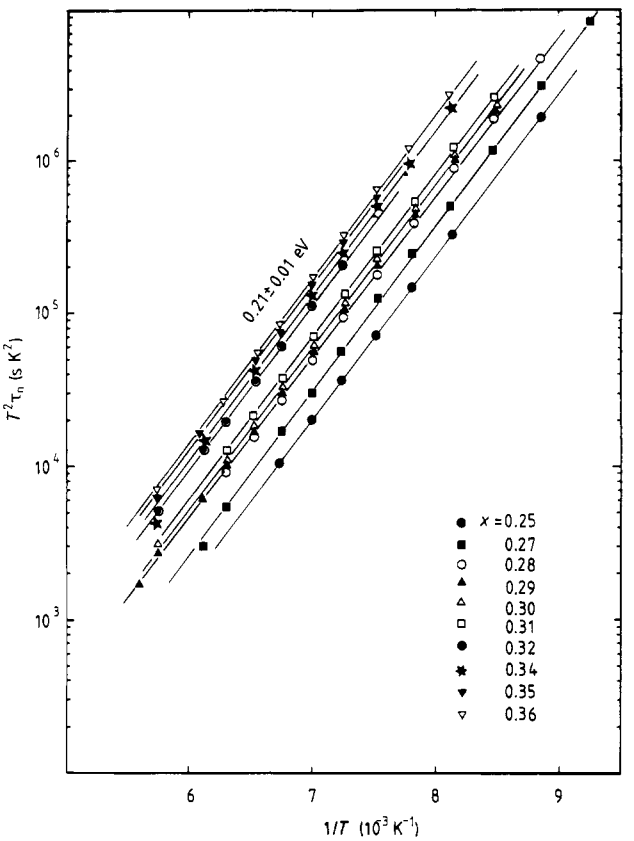

Figure 5. Temperature dependence of the emission time constant for the D–X centre electron traps in LPE $Al_xGa_{1-x}As$ in the direct band-gap range.

The value of ε_n decreases from $2.0\times10^3\,s^{-1}\,K^{-2}$ for $x=0.25$ to $0.6\times10^2\,s^{-1}\,K^{-2}$ for $x=0.36$.

Capacitance–voltage data were obtained under trap-empty and trap-full conditions by appropriately varying the bias and cycling the temperature. Plots of $V_e^{1/2}$ against C_W^{-1} for various values of x, obtained from measurements at 100 K are shown in figure 6. From a regression analysis of this data, values of trap depth E_T are obtained, and these are listed in table 1. Values of the emission activation energy ΔE_e and the difference $\Delta E_e - E_T$ are also listed in table 1.

The plots of the capture constant c against inverse temperature for $Al_xGa_{1-x}As$ with $x=0.25$, 0.29, 0.32 and 0.36 are shown in figure 7(a). The capture constants were obtained on the basis of equation (7) from DLTS data. The thermal activation energies of the plots of c against $1/T$ are also shown in figure 7(a).

On comparing the values of E_T and ΔE_e for the electron traps in $Al_xGa_{1-x}As$ as given in table 1, it will be seen that the final states of the emission transitions cannot be in the Γ minimum. In fact, the difference between the values of E_T and ΔE_e is only slightly less than the Γ–L energy separation found for this composition range both from pressure measurements [30] and from a three-conduction-valley analysis of Hall effect data for the same crystals. Moreover, the Hall effect studies yield values for E_T which are in excellent agreement with those derived from the C–V measurements using equation (1). It is, therefore, concluded that the traps in $Al_xGa_{1-x}As$ for $0.25\leqslant x\leqslant0.36$ are linked to, and emit electrons to the L valleys. Hence, $\Delta E_e - E_T = \Delta E_{L\Gamma} + \Delta E_B$; these values are listed in table 1. The emission cross sections, σ_∞^c, for the electron traps are also listed in table 1 and are found to decrease monotonically with increasing AlAs content.

If it is assumed that the traps in $Al_xGa_{1-x}As$ capture carriers from the L valleys for $0.25\leqslant x\leqslant0.36$, the capture constant c may be expressed as

$$c=\sigma^c v_T^L n_L, \tag{8}$$

where v_T and n_L are the thermal velocity and the concentration of electrons in the L valleys, respectively. Also, in the direct band-gap region, $n_L/n_\Gamma = (m_d^L/m_d^\Gamma)^{3/2}\exp(-\Delta E_{L\Gamma}/kT)$, where n_Γ is the concentration of electrons in the Γ valley. Furthermore, the approximation $n_\Gamma \simeq n_H$ is valid in the temperature range in which the capture constants were determined. $n_H(T)$ is the measured Hall carrier concentration and may be expressed as $n_H(T)=N_H\exp(-\Delta E_H/kT)$ in the temperature range of interest. ΔE_H is the effective thermal activation energy of $n_H(T)$ and N_H is the value of $n_H(T)$ for $T\rightarrow\infty$. The activation energy of a plot of c against $1/T$ as in figure 7(a), according to equation (8), is equal to $(\Delta E_H + \Delta E_{L\Gamma} + \Delta E_B)$. Knowing ΔE_H, the values of $(\Delta E_{L\Gamma} + \Delta E_B)$ are obtained. These values are included in table 1. The good agreement between the values of

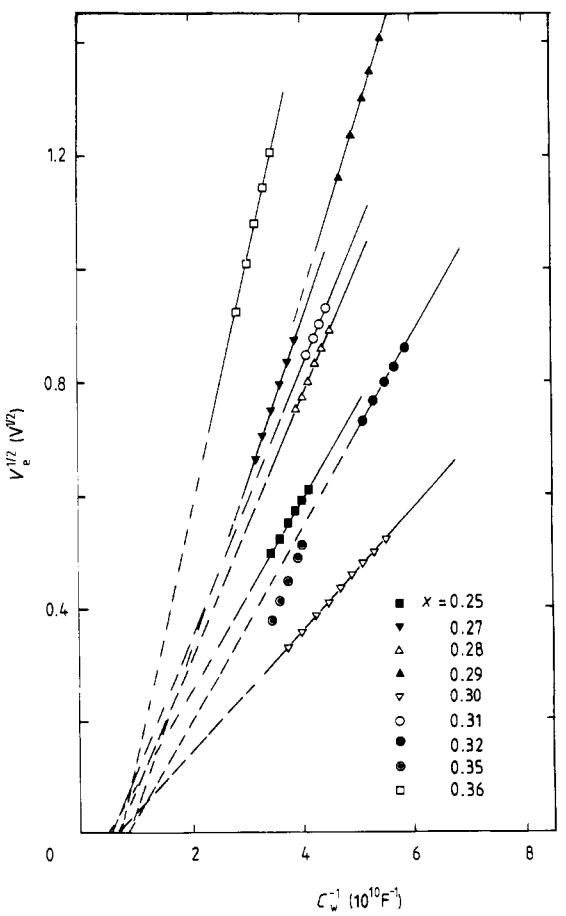

Figure 6. Plots of $V_e^{1/2}$ against inverse barrier capacitance, C_W^{-1}, for LPE $Al_xGa_{1-x}As$ with $0.25\leqslant x\leqslant0.36$. Extrapolation to $V_e=0$ yields C_L^{-1}.

Table 1. Parameters for electron trap in $Al_xGa_{1-x}As$ determined from analysis of *C–V* data, thermal emission and capture measurements.

AlAs content, x	E_T (eV)†	ΔE_e (eV)‡	$\Delta E_e - E_T = \Delta E_{L\Gamma} + \Delta E_B$ (eV)	$\Delta E_{L\Gamma} + \Delta E_B$ (eV)§	σ^e_∞ (10^{-19} cm^2)	σ^c_∞ (10^{-18} cm^2)
0.25	0.083	0.210	0.127	0.116	9.2	0.6
0.27	0.086	0.210	0.124	—	7.0	—
0.28	0.095	0.205	0.110	—	6.0	—
0.29	0.101	0.210	0.109	0.107	5.3	1.4
0.30	0.103	0.205	0.102	—	1.9	—
0.31	0.105	0.203	0.098	—	1.6	—
0.32	0.122	0.210	0.088	0.084	1.4	1.2
0.35	0.138	0.220	0.082	—	0.5	—
0.36	0.135	0.200	0.065	0.071	0.3	7.6

† Data obtained at 100 K.
‡ Data obtained from emission experiments.
§ Data obtained from carrier capture measurements.

$\Delta E_{L\Gamma} + \Delta E_B$ determined from independent emission and capture measurements should be noted.

The capture cross section for carrier capture, σ^c, was calcuated from the capture constants at different temperatures using equation (8). The values of m^L_c/m_0 used to determine v^L_T are the same as that used for carrier emission and the value of n_L was obtained from a three-conduction-valley analysis of Hall effect data. Fairly good agreement between σ^e_∞ and σ^c_∞ is obtained for $x = 0.25$ and 0.29. However, for $x = 0.32$ and 0.36, carrier capture via both the L and X valleys had to be included to improve the agreement between σ^e_∞ and σ^c_∞. The final values are listed in table 1 and the plots of σ^e against $1/T$ are displayed in figure 7(*b*). It is interesting to note that σ^e is thermally activated according to $\sigma^c = \sigma^c_\infty \exp(|\Delta E_B|/kT)$. An activation energy of $|\Delta E_B| \simeq 0.02$ eV is obtained from the slope of these plots, which is very small. The conduction band structure of $Al_xGa_{1-x}As$, the position of the L minima as obtained from analysis of Hall effect data and the trap energy depth E_T as obtained from analyses of capacitance data and Hall data are shown in figure 8.

The 0.21 eV electron trap in $Al_xGa_{1-x}As$ is next discussed. The data of figure 8 indicate that there is an

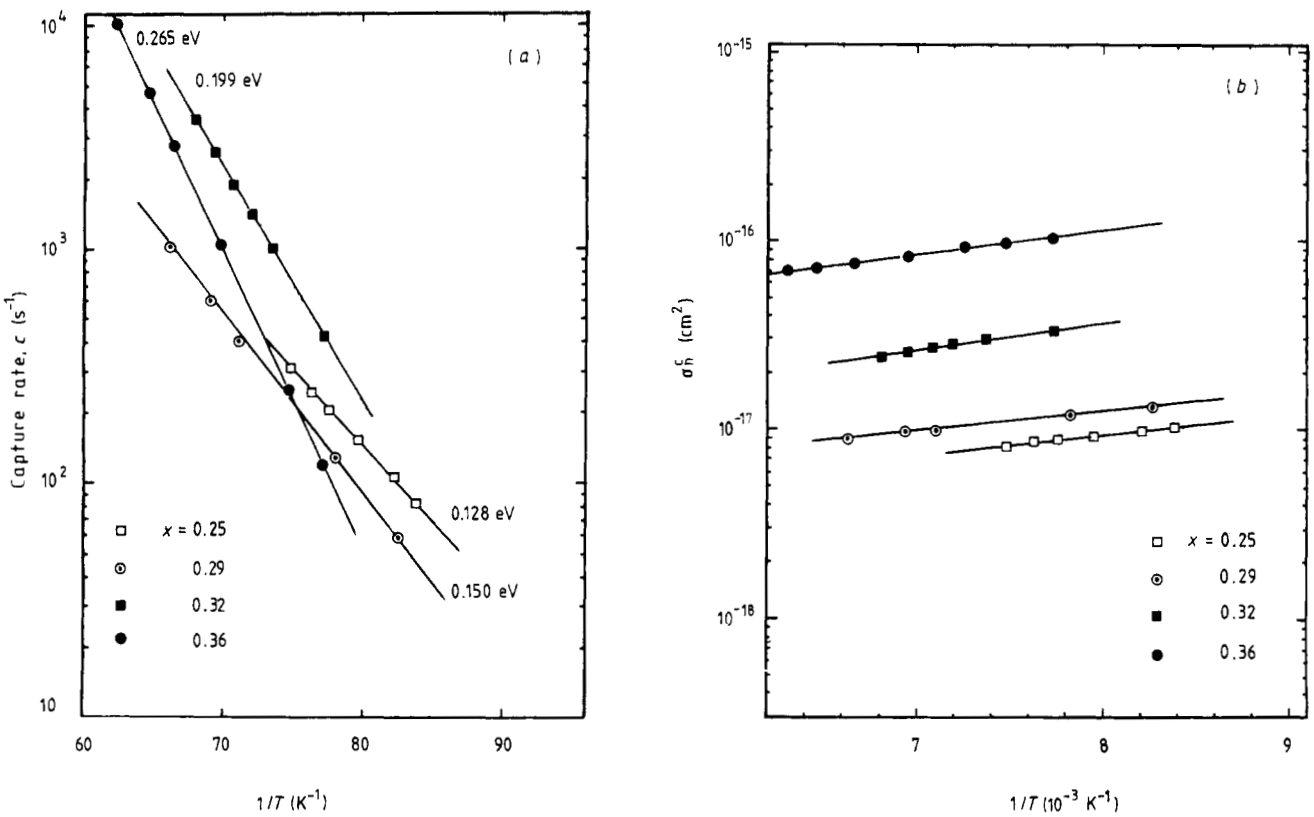

Figure 7. Results obtained from DLTS capture measurements on $Al_xGa_{1-x}As$. (*a*) Capture constant against inverse temperature; (*b*) electron capture cross section as a function of inverse temperature.

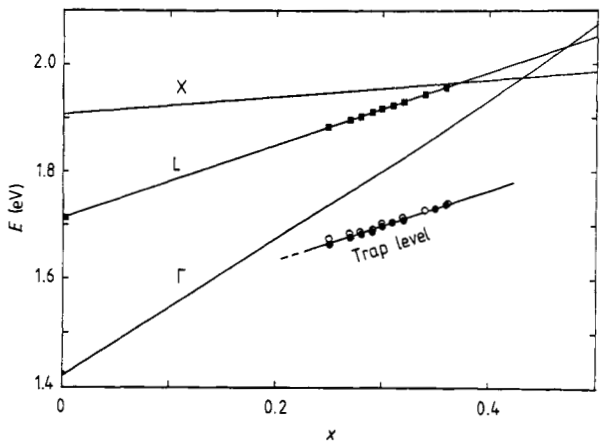

Figure 8. The conduction band structure and the energy position of trap levels in $Al_xGa_{1-x}As$ at 300 K. (●) From analysis of *C–V* data; (■) and (○) from analysis of temperature dependence of Hall carrier density ([17] and [29]).

excellent agreement, for nine different crystal compositions, between the energy level depth of the trap deduced from thermal equilibrium Hall effect measurements and from the *C–V* results interpreted on the basis of equations (1), (2) and (3). The energy variation of the L minima determined from analysis of these data are in excellent agreement with previous data, shown in figure 1; the values of $\Delta E_{L\Gamma}$ are identical to those obtained from hydrostatic pressure studies on the same crystals [30]. It is seen that the trap levels appear to be rigidly linked to the L minima. In view of the emission and capture results presented here, it must be concluded that these traps emit to and capture carriers from the indirect L minima and not from the lowest-lying Γ minimum. The capture constant c exhibits a strong temperature dependence (figure 7(*a*)). A similar result has been reported by Lang and Logan [31], who attribute the temperature dependence to an energy barrier associated with the capture cross section arising from a multi-phonon emission process; this interpretation leads to extremely small capture cross sections $\simeq 10^{-30}\,cm^2$. On the contrary, here the temperature dependence is explained in simple terms as resulting from the temperature dependence of the electron density in the L and X minima. Since the traps deionise below room temperature and thus strongly reduce the carrier concentration in the conduction band, the temperature dependence of the Γ conduction electrons has to be taken properly into account. As described in §2 these $Al_xGa_{1-x}As$ crystals show persistent photoconductivity at low temperatures. On the basis of the proposed model of emission and capture via the L minima, this effect can be explained as follows: at low temperature, after photo-excitation, the carriers are trapped in the Γ minimum. The important effect of the upper valleys of the conduction band, which have a high density of states compared with the Γ minimum, on the properties of deep-level traps has been discussed by Jaros [32, 33]. His results may explain the strong interaction of the traps analysed in this work with the L minima. Finally, reasonable agreement has been obtained between the emission and capture cross sections, as should be expected from detailed balance considerations.

In the indirect band-gap range, the traps emit electrons to the lowest X minima and the binding energy of the levels obtained from analysis of Hall effect data were in good agreement with the thermal activation energies for $x \geqslant 0.44$. The activation energies decreased monotonically for $x > 0.37$ to a value of 0.108 eV at $x = 0.78$ and are listed in table 2. If the electrons in the trap levels associated with the L and X conduction minima are assumed to be tightly bound to the ion cores, then, proceeding from the tight-binding approximation, a rather simple formulation may be made from which the binding energy of the electron trap levels may be estimated. The large density of states in these minima justify, to some degree of approximation, such a formulation which leads to:

$$\det \begin{vmatrix} E_X - E_{trap} & V_i \\ V_i & E_L - E_{trap} \end{vmatrix} = 0 \qquad (9)$$

where V_i is the pseudopotential or interaction potential of the traps at the L–X crossover point. Taking V_i equal to the measured binding energy of the level at the L–X band crossover composition ($x = 0.37$), and appropriate values for E_L and E_X, the energy positions of the defect levels below the conduction and minima can be calculated. This energy profile is indicated by the broken line in figure 1. The agreement between experimental and theoretical trap binding energies for large values of x suggests that the level is associated to some extent with the L valleys even when the X valleys are the lowest. The discrepancy for $x \leqslant 0.4$ is possibly because of a greater dominance of the electron wavefunctions in the Γ minimum, which has been ignored in the simple analysis.

The two main results derived from the trap emission and capture studies are the association of the traps with the indirect L and X minima and the non-existence of

Table 2. Parameters of electron traps in $Al_xGa_{1-x}As$ obtained from transient capacitance and Hall measurements.

AlAs content, x	ΔE_e (eV)†	ΔE_H (eV)‡	$\sigma_\infty^{el}(10^{-21}\,cm^2)$†
0.37	0.186	0.194	16.0
0.40	0.174	—	3.4
0.43	0.160	—	3.0
0.44	0.155	—	2.8
0.46	0.153	0.155	2.3
0.50	0.145	—	1.0
0.51	0.141	—	0.4
0.61	0.118	0.115	0.1
0.78	0.107	0.093	0.06

† Data obtained for emission experiments.
‡ Data obtained from analysis of temperature-dependent Hall data: this work ($x = 0.37$ and 0.46) and [17] ($x = 0.61$ and 0.78).

an activation barrier associated with the thermal capture cross section. The latter, in reality, leads to the conclusion that the lattice-relaxation of the D–X centres may be small, or near-zero. It may be mentioned that in Sn-doped $Al_xGa_{1-x}As$ the thermal energy barrier to capture has been found to be zero [34]. Results from other studies seem, to agree with these observations. The association of the traps with the L and X minima has been established by Saxena [35, 36] from hydrostatic pressure-dependent measurements on undoped crystals. More recently, Calleja *et al* [37] have made the same inference from data obtained from pressure-dependent studies on Si-doped AlGaAs. Tachikawa *et al* [38] have calculated the dependence of the D–X centre concentration on composition and hydrostatic pressure in AlGaAs, using a model in which the donor level associated with the L conduction band behaves as the D–X centre. The calculated electron occupancy in the D–X centre agrees quite well with experimental results. In fact, these authors have predicted the possibilities, based on the band structures, of the presence of the D–X centre in many other alloys. Some experimental data obtained by us from measurements on $In_{1-x}Al_xAs$/InP will be presented in the next section. Talwar *et al* [39] have made tight-binding calculations to study the local structure of the isolated Si impurity in GaAs and AlAs and have fitted their data to photo-ionisation cross section data reported by Henning and Ansems [40]. The fits lend support to a small lattice relaxation model. In conclusion, it may be said, with some caution that the lattice coupling of these defects is dependent on dopant species and concentration and certainly needs further investigation.

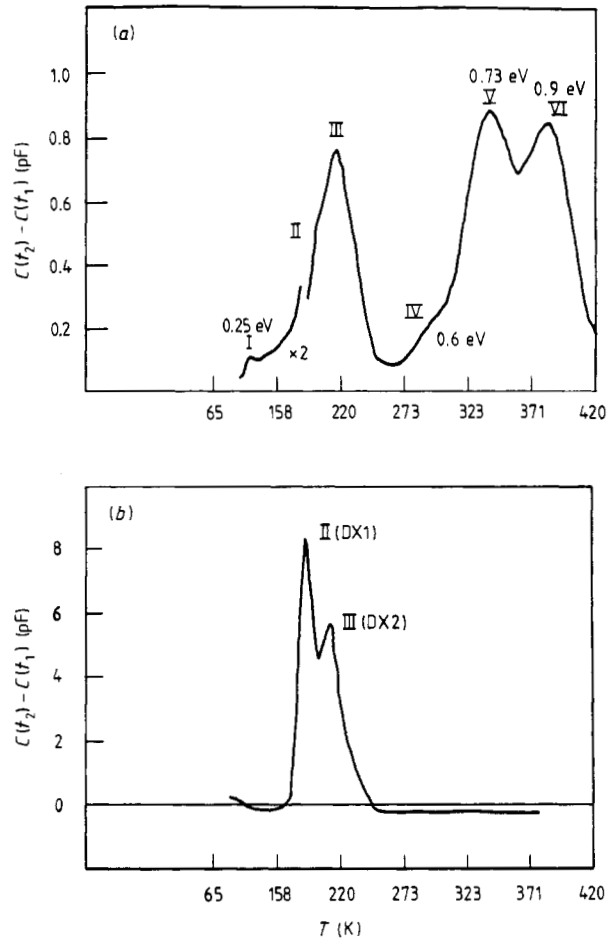

Figure 9. Typical DLTS data obtained from two Si-doped MBE grown $Al_xGa_{1-x}As$ samples with different values of x and the free-carrier concentration, n. (*a*) With $x=0.27$, $n=1.2\times10^{16}$ cm$_{-3}$ and $V_{rev}=-4.0$ V, showing all the traps present in Si-doped $Al_xGa_{1-x}As$. (*b*) With $x=0.29$, $n=1\times10^{18}$ cm^{-3} and $V_{rev}=-2$ V, showing DX1 and DX2 centres separately [41].

4. Multiplicity of D–X centres

Measurements were made with Schottky diodes made on molecular beam epitaxial (MBE) Si-doped $Al_xGa_{1-x}As$ grown in our laboratories [41]. Typical data [41] obtained from conventional constant-bias DLTS measurements on $Al_xGa_{1-x}As$ are shown in figure 9(*a*). At this point, the origins of the deep centres, except those labelled II and III, are largely unknown. There is some evidence that the 0.73 eV trap (V) at high temperatures may be related to a lattice vacancy or to an antisite [42, 43], but this is to be confirmed. Trap VI is also characteristic of samples grown at low temperatures [44], as is the case in this study. But the traps of primary interest here are those labelled II and III which are seen more clearly in figure 9(*b*) for a sample with high Si doping. Both have characteristics similar to the D–X centre in Si-doped $Al_xGa_{1-x}As$ [11, 12], and we believe they are related. The difference in thermal ionisation energy ΔE_e of the two centres, determined from the Arrhenius plots of figure 10 is 40–45 meV. This is almost equal to the splitting of the L donor state due to inter-valley scattering and the resulting valley–orbit splitting [45]. This lends further evidence to the fact that the centres are predominantly

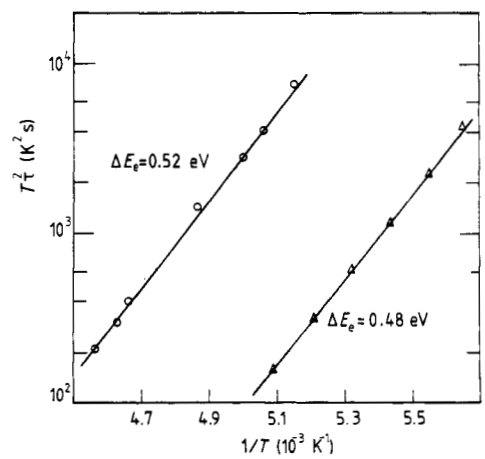

Figure 10. Temperature-dependent emission data for the two levels (△) DX1 and (○) DX2 identified in MBE grown Si-doped $Al_xGa_{1-x}As$. The measured activation energies, ΔE_e, are indicated.

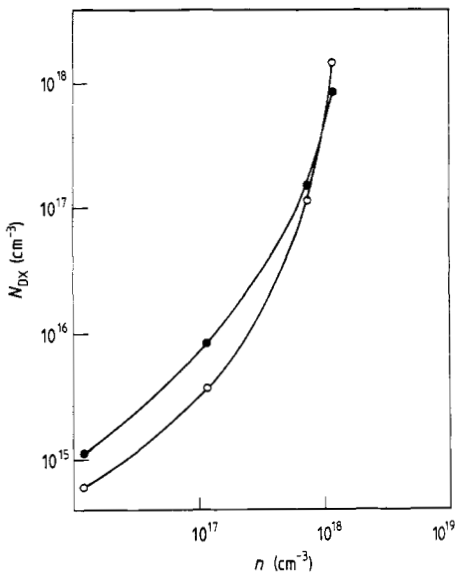

Figure 11. Variation of the concentrations of (○) DX1 and (●) DX2 centres in Si-doped MBE $Al_{0.29}Ga_{0.71}As$ as a function of free carrier concentration n.

coupled to the L minima, and that there are two (or more) closely-coupled D–X centres forming a 'family'. It should be pointed out that the exact energy values may be in slight error due to large trap densities and field-induced emission effects that are associated with conventional DLTS measurements. It may also be mentioned that the presence of two closely related electron traps in MBE and LPE $Al_xGa_{1-x}As$ has been detected by other authors [38, 45–47].

The centration of the two centres as a function of Si doping is shown in figure 11. It is seen that the concentration of DX1 (trap II) is lower than that of DX2 (trap III) at lower Si doping levels, and the reverse is true for high doping levels. It should be reiterated that these deep-donor centres are present in addition to a shallow hydrogenic donor whose concentration is insignificant compared with that of the DX centres at high doping levels. Some authors [45] point out that the shallow level changes to the D–X centre for $x > 0.24$. This may not be true in view of our Hall effect data and of earlier work by Saxena [35] and Chand *et al* [48].

5. D–X centres in other III–V alloy systems

$In_{0.52}Al_{0.48}As$, lattice-matched to InP is an important ternary alloy which is being used in a number of electronic and optoelectronic devices. The first experimental study of deep level traps in this alloy was made in [49]. DLTS measurements were made on $In_{0.52}Al_{0.48}As$ doped n- and p-type with Si and Be, respectively. Four electron traps and four hole traps were identified. The characteristics of the traps were not similar to the D–X centres in $Al_xGa_{1-x}As$. Moreover, Hall measurements on the same crystals did not show any persistent photoconductivity. One may then ask the question of whether the centres can be present in compositions close to the lattice-matched ones. On observing the conduction band structure of the $In_{1-x}Al_xAs$ ternary system [38], it is seen that, for Al content >55%, the L and X minima are lower in energy than the Γ minimum. It is, therefore, of interest to investigate these compositions for possible existence of the D–X centre.

DLTS measurements were performed [49] on $In_{1-x}Al_xAs$ samples with $0.48 < x \leq 0.57$. These were either grown directly on the InP substrates or with a suitable graded buffer layer, starting with the lattice-matched composition. Arrhenius plots of two new electron traps, ES1 and ES2, observed in the directly grown mismatched alloy, of one composition in the above range, are shown in figure 12. Note that the extrapolated capture cross sections σ_∞ are $\simeq 10^{-17}$–10^{-18} cm^2. It was also observed that the density of ES1 increased in the range 10^{15} to 10^{16} cm^{-3} with increase in Si-doping level. The ES2 level did not show this trend. On the other hand, the peak labelled ES2 was almost absent ($N_T < 10^{15}$ cm^{-3}) in the layers grown with a buffer layer. This indicates that the trap ES2 is related to strain in the ternary layer. The persistent photoconductivity (PPC) behaviour in the samples was studied by cycling the temperature of a Schottky diode and measuring the capacitance under different bias and temperature conditions, as was done with $Al_xGa_{1-x}As$. A large PPC effect was observed in samples in which only ES1, or in which both ES1 and ES2, were present. By measuring the amount of incremental photocapacitance, it is found that the PPC is due to trap ES1 in samples in which both ES1 and ES2 are present. In view of a small σ_∞, strong dependence on Si-doping and the observed PPC, it can be said, with some caution, that the ES1 trap has properties similar to the donor-related D–X centre in $Al_xGa_{1-x}As$. It is worthwhile to mention that Nojima and co-workers [50] have made DLTS measurements on InGaAlP alloys in which the L minima are lowest in

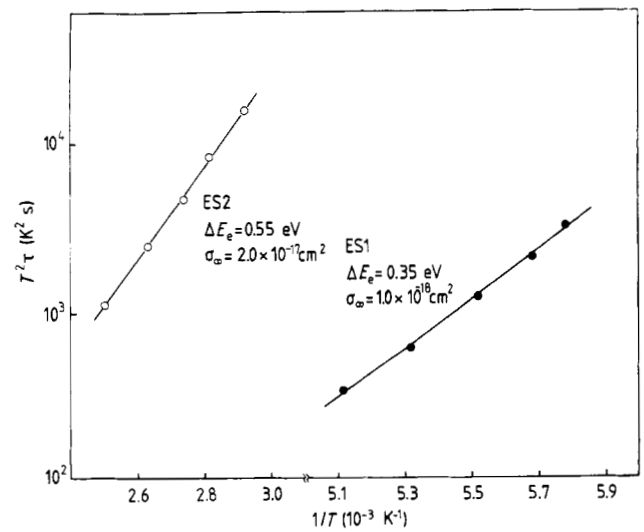

Figure 12. Temperature dependence of the emission time constant of electron traps in strained $In_{0.43}Al_{0.57}As$ on InP, in which the indirect L minima are lowest in energy. Traps ES1 exhibits properties similar to the D–X centre in $Al_xGa_{1-x}As$.

energy, and they have identified a trap which also exhibits properties similar to the D–X centre.

6. Concluding remarks

It is clearly obvious that the dominant D–X centres, first observed in the $Al_xGa_{1-x}As$ alloys, are a class of defects with unique thermal and optical kinetic properties. The detailed microscopic structure of the defect is still unclear. Assignments range from an impurity–vacancy complex, originally proposed by Lang [10], to a simple substitutional donor defect, proposed by Mizuta *et al* [45]. In this paper I have reviewed and described the other important aspect of the D–X centres—their relationship with the conduction band structure, and, in particular, their association with the indirect L and X minima in $Al_xGa_{1-x}As$. It is shown that taking this fact into account the observed thermal emission and capture properties can be consistently explained. The association of the traps with the indirect minima is also indirectly evident from the observed multiplicity of the levels. Finally, it is seen that in the $In_{1-x}Al_xAs$ alloys grown on InP, traps behaving exactly like the D–X centres emerge once the L minima are lowest in energy in the conduction band structure. Similar results have also been reported in the InGaAlP alloys. It is, therefore, important to recognise this important physical property of these unique defects and use it as a basis for a model for its microstructure.

Acknowledgment

The work was partly supported by the Department of Energy under grant DE-FG02-86ER45250.

References

[1] Mead C A and Spitzer W G 1963 *Phys. Rev. Lett.* **11** 358
[2] Stukel D J and Euwema R N 1969 *Phys. Rev.* **188** 1193
[3] Casey H C and Panish M B 1969 *J. Appl. Phys.* **40** 4910
[4] Lorenz M R, Chicotka R, Pettit G D and Dean P J 1970 *Solid State Commun.* **8** 693
[5] Onton A, Chicotka R J and Yacoby Y 1972 *Proc. 11th Int. Conf. Physics of Semiconductors (Warsaw) 1972* unpublished p 1023
[6] Dingle R, Logan R A and Arthur J R 1977 *Gallium Arsenide and Related Compounds (Edinburgh) 1976* (Inst. Phy. Conf. Ser. 33a) p 210
[7] Bhattacharya P K, Owen S J T and Marrs J 1980 *Appl. Phys. Lett.* **36** 664
[8] Aspnes D E, Kelso S M, Logan R A and Bhat R 1986 *J. Appl. Phys.* **60** 754
[9] Keuch T F, Wolford D J, Potemski R, Bradley J A, Kelleher K H, Yan D, Farrell J P, Lesser P M S and Pollack F H 1987 *Appl. Phys. Lett.* **51** 505
[10] Lang D V, Logan R A and Jaros M 1979 *Phys. Rev.* B **19** 1015
[11] Lang D V and Logan R A 1979 *Physics of Semiconductors 1978* (Inst. Phys. Conf. Ser. 43) p 433
[12] Kumagai O, Kawai H, Mori Y and Kaneko K 1984 *Appl. Phys. Lett.* **45** 1322
[13] Narayanamurti V, Logan R A and Chin M A 1979 *Phys. Rev. Lett.* **43** 1536
[14] Petroff P M, Lang D V, Logan R A and Johnston W D 1978 *Defects and Radiation Effects in Semiconductors 1978* (Inst. Phys. Conf. Ser. 46) p 427
[15] Stormer H L, Dingle R, Gossard A C, Wiegmann W and Sturge M D 1979 *Solid State Commun.* **29** 705
[16] Panish M B 1973 *J. Appl. Phys.* **44** 2667
[17] Saxena A K 1979 *Phys. Status Solidi* b **96** K77
[18] Nelson R J 1977 *Appl. Phys. Lett.* **31** 351
[19] SpringThorpe A J, King F D and Becke A 1975 **4** 101
[20] Saxena A K 1980 *Appl. Phys. Lett.* **36** 79
[21] Kaneko K, Ayabe M and Watanabe N 1977 *Gallium Arsenide and Related Compounds (Edinburgh) 1976* (Inst. Phys. Conf. Ser. 33a) p 216
[22] Balland B, Vincent G, Bois D and Hirtz P 1979 *Appl. Phys. Lett.* **34** 108
[23] Gaj J A, Majerfeld A and Pearson G L 1971 *Phys. Status Solidi* b **48** 513
[24] Metz S and Fritz W 1977 *Gallium Arsenide and Related Compounds (Edinburgh) 1976* (Inst. Phys. Conf. Ser. 33a) p 66
[25] Metz S 1978 *Appl. Phys. Lett.* **33** 198
[26] Lang D V, Logan R A and Kimmerling L C 1976 *Proc. 13th Int. Conf. Physics of Semiconductors (Rome) 1976* unpublished p 615
[27] Majerfeld A and Bhattacharya P K 1978 *Appl. Phys. Lett.* **33** 259
[28] Lang D V 1974 *J. Appl. Phys.* **45** 3023
[29] Bhattacharya P K, Majerfeld A and Saxena A K 1979 *Gallium Arsenide and Related Compounds 1978* (Inst. Phys. Conf. Ser. 45) p 199
[30] Sugeta T, Majerfeld A, Saxena A K and Robson P N 1977 *Appl. Phys. Lett.* **31** 842
[31] Lang D V and Logan R A 1977 *Phys. Rev. Lett.* **39** 635
[32] Jaros M 1975 *J. Phys. C: Solid State Phys.* **8** L264
[33] Jaros M 1975 *J. Phys. C: Solid State Phys.* **8** 2455
[34] Lang D V and Logan R A 1979 *Physics of Semiconductors 1978* (Inst. Phys. Conf. Ser. 43) p 433
[35] Saxena A K 1980 *J. Phys. C: Solid State Phys.* **13** 4323
[36] Saxena A K 1981 *Phys. Status Solidi* b **105** 777
[37] Calleja E, Gomez A and Munoz E 1988 *Appl. Phys. Lett.* **52** 383
[38] Tachikawa M, Mizuta M and Kukimoto H 1984 *Japan. J. Appl. Phys.* **23** L1594
[39] Talwar D N, Manasreh M O, Suh K S and Covington B C 1987 *Appl. Phys. Lett.* **51** 1358
[40] Henning J C M and Ansems J P M 1987 *Semicond. Sci. Technol.* **2** 1
[41] Dhar S, Hong W-P, Bhattacharya P K, Nashimoto Y and Juang F-Y 1986 *IEEE Trans. Electron Devices* **ED-33** 698
[42] Naritsuka S, Yamanaka K, Mihara M and Ishii M 1984 *Japan J. Appl. Phys.* **23** L112
[43] Yamanaka K, Naritsuka S, Mannoh M, Yuasa T, Nomura Y, Mihara M and Ishii M 1984 *J. Vac. Sci. Technol.* B **2** 229
[44] McAfee S R, Tsang W T and Lang D V 1981 *J. Appl. Phys.* **52** 6165

[45] Mizuta M, Tachikawa M, Kukimoto H and Minomura S 1985 *Japan. J. Appl. Phys.* **24** L143
[46] Zhou B L, Ploog K, Gmelin E, Zheng X Q and Schulz M 1982 *Appl. Phys.* A **28** 223
[47] Ohno H, Akatsu Y, Hashizume T and Hasegawa H 1985 *J. Vac. Sci. Technol.* B **3** 943 1985
[48] Chand N, Fischer R, Klem J, Henderson T, Pearah P, Masselink W T, Chang Y-C and Morkoc H 1985 *J. Vac. Sci. Technol.* B **3** 644
[49] Hong W-P, Dhar S, Bhattacharya P and Chin A 1987 *J. Electron. Mater.* **16** 271
[50] Nojima S, Tanaka H and Asahi H 1986 *J. Appl. Phys.* **59** 3489